THE JOURNAL OF PHYSICAL CHEMISTRY B

Article

pubs.acs.org/JPCB

Computational Studies of the Regioselectivities of COMT-Catalyzed *Meta*-/*Para*-O Methylations of Luteolin and Quercetin

Yang Cao, Zhong-Jian Chen, Hui-Di Jiang, and Jian-Zhong Chen*

Institute of Materia Medica, College of Pharmaceutical Sciences, Zhejiang University, Hangzhou, Zhejiang 310058, P. R. China

Supporting Information

ABSTRACT: Catechol-*O*-methyltransferase (COMT, EC 2.1.1.6) plays a central role in the inactivation of neurotransmitters sharing a catecholic motif by transferring a methyl group from AdoMet. Methylation of the *meta*-hydroxyl is much more common than that of the *para*-hydroxyl in many COMT substrates, such as dopamine and norepinephrine. Our experimental data showed that quercetin preferred *meta*-methylation but luteolin favored a *para*-methylation. To elucidate the mechanism for different preferences of methylations of quercetin and luteolin, we performed a theoretical investigation on the different regioseletivities of COMT-catalyzed methylations for quercetin and luteolin by a combined approach of MD simulations, *ab initio* calculations, and QM/MM computations. The *ab initio* calculation results showed that both quercetin and luteolin have more negative charge distributions on the *meta*-O atom than the *para*-O atom, which indicated that *meta*-O preferred S_N2 reaction for their methylation. Our QM/MM computations also confirmed that these two flavonoids have lower reaction energetic barriers for COMT-catalyzed *meta*-O-methylation than *para*-O-methylation. On the other hand, our binding free energy computation results indicated that quercetin has a more stable binding mode for *meta*-O-methylation than *para*-O-methylation but luteolin has a more stable binding mode for *para*-O-methylation than *meta*-O-methylation. We gave a comprehensive explanation considering both thermodynamics and reaction kinetics aspects and discussed the protein−inhibitor interactions as well as the O-methylation mechanism in our present work.

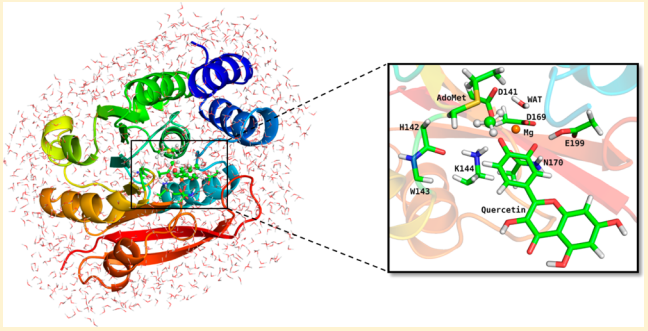

INTRODUCTION

The monomeric protein catechol-*O*-methyltransferase (COMT; EC 2.1.1.6) is a primary enzyme to deactivate catecholamine neurotransmitters, including dopamine, norepinephrine, and epinephrine through enzymatic O-methylation of a single hydroxyl group in a catecholic motif.[1] There are two isoforms of COMTs in the human body, namely, the soluble COMT (S-COMT) and the membrane-bound COMT (MB-COMT). S-COMT is present as the vast majority in peripheral tissues, and MB-COMT exists mainly in the human brain. Both human S-COMT and MB-COMT are coded by one single gene using two separate promoters,[2] and MB-COMT has an additional 50 amino acids at the N-terminal for its anchor on the cell membrane. As the level of catecholamines is reduced in a number of medical conditions, such as Parkinson's disease, several pharmaceutical drugs targeting COMT were designed to alter its activity and therefore to increase the availability of catecholamines.[3] The substrates of COMT include catecholestrogens, xenobiotic inhibitors, and flavonoids, all of which contain a common catechol motif in their structure.

Crystallographic and theoretical studies have provided direct and detailed insights into the binding mode and catalytic mechanism of COMT particularly in the case of nitro-substituted catechol derivatives and catecholamines.[4−8] Lotta et al.[9] elucidated an ordered binding process beginning with the insertion of the methyl donor *S*-adenosyl-L-methionine (AdoMet) to COMT, followed by a divalent magnesium ion and then the catecholic substrate. Depending on which hydroxyl group on the catecholic motif orientates toward the methyl donor of AdoMet, COMT could catalyze the substrate to form two different methylates (*meta*-O-methylation or *para*-O-methylation relative to the substituent on the catechol ring) via an S_N2 displacement reaction (Scheme 1). *In vitro*, the enzyme has been proved to have a preference of undertaking *meta*-O-methylation especially when toward catecholamines.[10,11] The regioselectivity is believed to be mainly determined by the polarity and orientation of the substituents, while the nucleophilicity of the catechol-O plays a lesser role.[11,12]

Flavonoids containing a catecholic group are widely distributed in edible fruits and vegetables.[13] This family has received widespread attention with their extensive pharmacological activities, such as antioxidant, antiosteoporotic, and anti-inflammatory properties.[14,15] In general, flavonoids are metabolized by glucuronidation promoted by uridine-5-diphosphate glucuronosyl transferases (UGTs) or sulfation

Received: October 17, 2013
Revised: December 18, 2013
Published: December 19, 2013

Scheme 1. Two Different Methylation Reactions

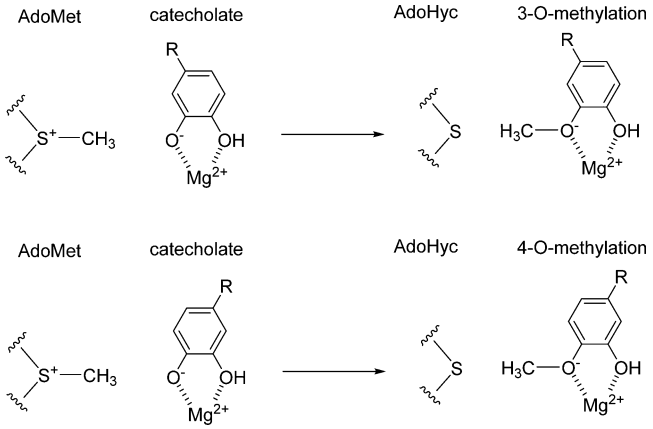

catalyzed by sulfotransferases (STs) *in vivo*. On the other hand, it was also demonstrated that the flavonoids containing the catechol moiety, such as quercetin (3,3′,4′,5,7-pentahydroxyflavone) and luteolin (2-(3,4-dihydroxyphenyl)-5,7-dihydroxy-4*H*-chromen-4-one), are also methylated by COMT.[16,17] Because of the wide distribution of COMT in human and rodent tissues,[5] like liver, intestine, lung, brain, and platelet,[18] there is no doubt that the methylation is essential in the disposition of these catecholic flavonoids.

Our recent metabolism studies[19] of luteolin's methylation by recombinant human S-COMT *in vitro* showed that luteolin favors a *para*-O-methylation, with a ratio of *meta*-/*para*-production in V_{max}/K_m of 0.703 (Table 1 and Figure S1a in the Supporting Information), which is contrary to the general factor of known substrates of COMT.[20] Alternatively, our further experimental data indicated that the V_{max}/K_m ratio of *meta*-/*para*-production turned out to be approximately 3 in the case of quercetin (Table 1 and Figure S1b in the Supporting Information). That means that luteolin and quercetin have differently preferable COMT-promoted methylation at the positions of 3′-OH and 4′-OH. By comparing the structures of luteolin and quercetin, it can be seen that quercetin has one more hydroxyl group substituted on the C3 position than luteolin. How does the structure of flavonoid affect the regioselectivity of its methylation catalyzed by COMT, and what is the key factor that reverses the relative preference of *meta*-O-methylation and *para*-O-methylation metabolites?

Theoretical computations have been reported to study the structural mechanism of COMT involved methylations of catecholic compounds. For example, the binding free energy calculations[21] without entropy contributions showed that human COMT would favorably proceed to form the 3′-O-methylation product over the 4′-O-methylation for the compound catechin based on 70 ps molecular dynamics (MD) simulations. The empirical docking[22] was carried out to explain the difference in *meta*/*para* selectivity between the methylation of catechins and procyanidins. MD simulations[12] were performed to provide the structural explanation for the observed preference of *meta*-O-methylated products over *para*-O-methylated products. QM/MM optimizations[23] were implemented to obtain a transition structure of catecholate located in the active site of COMT. However, these computational studies did not really resolve the structural mechanism for the regioseletivity of flavonoid's methylation catalyzed by COMT. Alternatively, it could be assumed that the regioselectivity of COMT-catalyzed O-methylation of catechol would be controlled by both the binding free energy of substrate binding to its target enzyme and the energetic barrier of enzyme-catalyzed reaction on the basis of these studies.

In the present work, we focused our attention on a structurally mechanistic investigation of different regioslectivities of COMT-catalyzed O-methylations on the catechol group of the two flanovoids quercetin and luteolin by theoretical computations. In general, the binding affinity of the substrate within the active pocket of protein will be the first key point that may be regarded as the thermodynamics factor for its methylation. The second key point, known as the reaction kinetics factor, would be that the complex of substrate binding to enzyme should overcome the reaction barrier to generate the product. The regioselectivity is assumed to be mainly impacted by these two aspects. In fact, Palma et al.[4] has identified the major structure and chemical factors that determine the enzyme's regioselectivity of O-methylation toward nitrated inhibitors in both thermodynamics and reaction kinetics perspectives.

Molecular mechanics/Poisson−Boltzmann surface area (MM/PBSA)[24] and molecular mechanics/generalized Born surface area (MM/GBSA)[25] are indeed specific for the free-energy calculations for a ligand binding to its target protein by integrating molecular mechanics energy and continuum solvation models. We predicted the binding affinities of either quercetin or luteolin, with different conformations and orientations, docking into the binding pocket of COMT by applying a combined computational approach of MD simulation, MM/PB(GB)SA free energy calculations, and free energy decomposition analyses. The computational results would help us to identify the preferred conformation and orientation of quercetin or luteolin binding to COMT for their 3′-O-methylations or 4′-O-methylations. In addition, we analyzed the interaction features between COMT and each flavonoid to understand the specificity of its binding to COMT according to the MD simulated structural models. On the basis of the MD simulated structural models of COMT-AdoMet-quercetin-Mg^{2+} or COMT-AdoMet-luteolin-Mg^{2+}, the hybrid quantum mechanics/molecular mechanics (QM/MM) ap-

Table 1. Kinetic Parameters for Formation of *meta*- and *para*-Methylated Luteolin/Quercetin in Incubation with Recombinant Human COMT[a]

	luteolin		quercetin	
parameter	*meta*-MeO	*para*-MeO	*meta*-MeO	*para*-MeO
V_{max} (nmol mg protein^{-1} min^{-1})	0.784 ± 0.044	1.17 ± 0.082	0.254 ± 0.032	0.108 ± 0.030
K_m (μM)	0.673 ± 0.097	0.706 ± 0.147	3.27 ± 0.529	4.21 ± 1.46
$CL_{int}(V_{max}/K_m)$ (mL mg protein^{-1} min^{-1})	1.19 ± 0.201	1.70 ± 0.32	0.0780 ± 0.0031	0.0260 ± 0.0017
(*meta*-/*para*-) of CL_{int}	0.703		3.03	

[a]Data are expressed as mean ± SD, n = 3.

dx.doi.org/10.1021/jp410296s | J. Phys. Chem. B 2014, 118, 470−481

proach[26−28] was applied to study the reaction energy barriers of COMT-catalyzed methylations. QM/MM calculations would help us to explore the reaction capability of two phenolic hydroxyls on the catecholic motif of the flavonoids in the enzymatic environment and to probe into the reaction kinetics factor which is also likely involved in influencing the regioselectivity. The theoretically computational result could help to propose a structural mechanism for the different regioselectivities of COMT-catalyzed O-methylations for the two flavonoids quercetin and luteolin.

COMPUTATIONAL DETAILS

Initial Structures Preparation. The conformations of either quercetin or luteolin were first generated by using the Sketch module of the SYBYL-X 1.3 molecular modeling software package.[29] As illustrated in Figure 1, two different

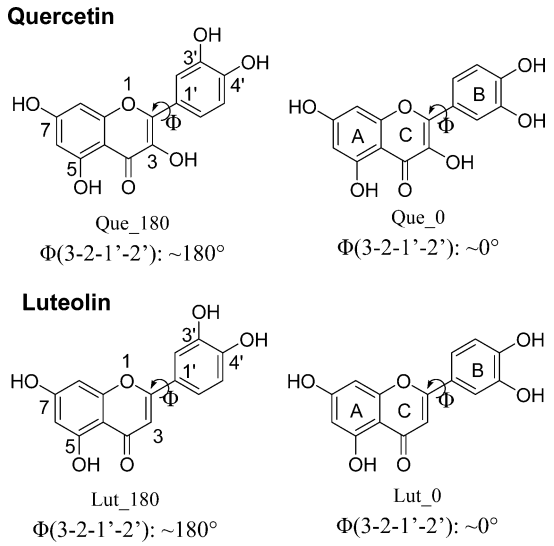

Figure 1. The two conformations of either quercetin or luteolin.

conformations, with dihedral angles Φ(3−2−1′−2′) near 0° (Lut_0 and Que_0) or 180° (Lut_180 and Que_180), were produced for either quercetin or luteolin, since these two conformations could be observed in their cocrystal structures with different proteins (PDB entries: 4HKN (Lut_0 binding to human tankyrase 2),[30] 4DGN (Lut_180 binding to casein kinase II),[31] 1H1I (Que_0 binding to quecetin 2,3-dioxygenase),[32] 2O3P (Que_180 binding to PIM1 kinase),[33]). Each *in silico* sketched conformation of either quercetin or luteolin was subjected to a full geometry optimization at the HF/6-31G* level of theory using the Gaussian 09 program.[34]

The X-ray cocrystal structure of human S-COMT bound with AdoMet, Mg^{2+}, and 3,5-dinitrocatechol, obtained from the Protein Data Bank (PDB entry: 3BWY[35]), was applied for the current theoretically computational studies. Each Gaussian-optimized conformation of quercetin or luteolin was superimposed with 3,5-dinitrocatechol on the catechol moiety to replace it for the generation of an initial structure model of the complex COMT-AdoMet-quercetin-Mg^{2+} or COMT-AdoMet-luteolin-Mg^{2+} by using the SYBYL-X 1.3 molecular model software package.[29] Our experimental data has demonstrated that the COMT-catalyzed methylation can happen at 3′-OH or 4′-OH, respectively, of either quercetin or luteolin. Therefore, there were eight starting systems constructed in parallel for MD simulations. These eight complexes were named as Que_180_*m*, Que_0_*m*, Que_180_*p*, Que_0_*p*, Lut_180_*m*, Lut_0_*m*, Lut_180_*p*, and Lut_0_*p*, respectively, in which "*m*" and "*p*" respectively stand for each flavonoid's binding mode with *meta*-OH or *para*-OH pointing to the CH_3−S group of AdoMet to be ready for the methylation. Figure 2 displayed Que_0_*m* and Que_180_*p* as representative diagrams of flavonoids' binding modes in COMT. The structural diagrams of other six complexes Que_180_*m*, Que_0_*p*, Lut_180_*m*, Lut_0_*m*, Lut_180_*p*, and Lut_0_*p* were shown in Figure S2 in the Supporting Information.

MD Simulations. Molecular dynamics simulations were performed on each of eight complexes, respectively, using the AMBER 11 software package.[36] Each complex was first solvated in a truncated octahedron box of TIP3P[37] water molecules with a margin distance of 9.0 Å to get the corresponding solvation system. The partial atomic charges for quercetin or luteolin and AdoMet were determined using the restrained electrostatic potential (RESP) protocol implemented in the ANTECHAMBER module of AMBER 11 through fitting the electrostatic potentials calculated by Gaussian 09[34] at the HF/6-31G* level of theory. Missing hydrogen atoms were added using the LEaP

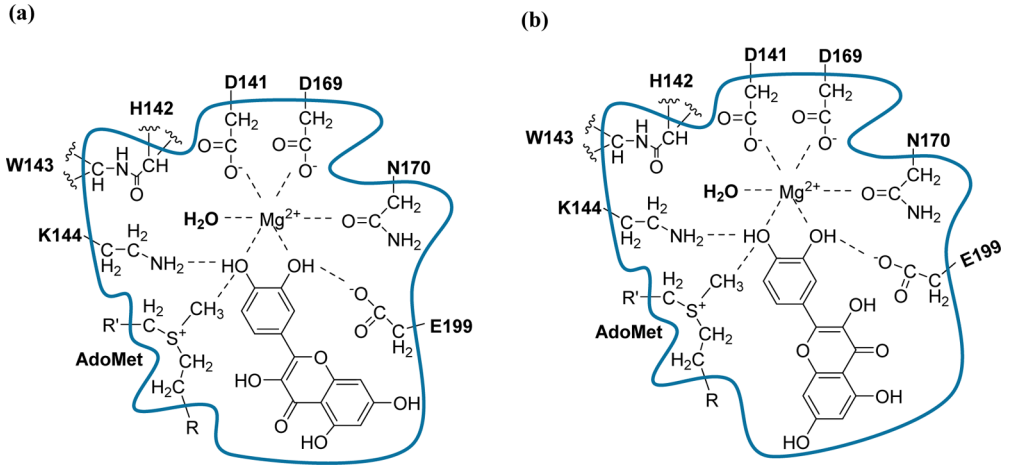

Figure 2. The (a) Que_180_*p* and (b) Que_0_*m* model systems considered for the MD simulations and QM/MM calculations. During the ONIOM computations, the atoms inside the box are treated as the QM layer, while the rest outside the box are set as the MM layer.

dx.doi.org/10.1021/jp410296s | J. Phys. Chem. B 2014, 118, 470−481

module[38] in AMBER 11. An additional six Na^+ ions were then added to neutralize the system. The general AMBER force field (GAFF)[39] was applied to describe the force field parameters of the substrates including quercetin or luteolin and AdoMet, while the AMBER ff99SB force field[40] was assigned to establish the potential of COMT, water molecules, and ions of Na^+ and Mg^{2+}.

Prior to the MD simulations, each system was subjected to three steps of energy minimizations conducted by the SANDER module in AMBER 11. First, all Na^+ and water molecules except the crystal water coordinated to Mg^{2+} were optimized. Second, the flavonoid, AdoMet, Mg^{2+}, the water molecule in the active site, and the protein backbone atoms were restrained with a constraint force of 5.0 kcal/mol·Å^2. Finally, the whole system was optimized without any restraint. In every step, structural optimization was implemented using 2500 steps of steepest descent followed by 5000 steps of the conjugate gradient method.

For the sake of examining the protonation states of the bound flavonoids' catechol moiety in the active center, we performed energetic scanning calculations of proton transfer from the catecholic hydroxyl group to the carboxyl group of COMT's Glu199 in the prepared eight complexes using the QM/MM approach (details of dividing the QM and MM regions and the level of theory applied will be discussed in the "QM/MM calculation" section). In each complex, the proton of the catechol moiety's hydroxyl group, which is far away from AdoMet, could automatically transfer to the carboxyl group of Glu199 during the energetic scanning calculations (Figure S3 in the Supporting Information), thus making Glu199 exist in the neutral form. Such a phenomenon could probably be caused by the presence of Mg^{2+} which lowers the pK_a of the hydroxyl group of catechol.[41] The protonated state of Glu199 was also shown to be more stable in a semiempirical study by Martti et al.[42] Likewise, Lys144 was predicted to act as the base to deprotonate the hydroxyl group of catechol before the rate-determining S_N2 methylation proceeded.[5] Herein, the anionic form of each flavonoid was assumed in the following MD studies.

Subsequently, every system was gradually heated in the NVT ensemble from 0 to 300 K over 100 ps with a force constant of 10.0 kcal/mol·Å^2 on all heavy atoms of flavonoid, AdoMet, Mg^{2+}, and the water molecule within COMT's active site and all backbone atoms of COMT. The whole system was then subjected to seven rounds of equilibration (50 ps each at 300 K) with a carefully reducing structural restraint of 10, 5, 3, 1, 0.5, 0.1, and 0 kcal/mol·Å^2, respectively, while the solvation environment was kept free. Finally, a 10 ns MD production run on each system with a periodic boundary condition in the NPT ensemble was carried out at 300 K with particle-mesh Ewald (PME)[43] employed to deal with the long-range electrostatic interactions. A 10 Å cutoff distance was used for the long-range van der Waals (vdW) energy term. The SHAKE algorithm[44] was employed to keep all bonds involving hydrogen atoms rigid. The trajectories were recorded every 1 ps.

Binding Free Energy Calculations. For each complex, 400 snapshots were extracted from the last 2 ns MD at 5 ps intervals to estimate the binding free energy of the corresponding conformation and binding pose of the flavonoid with human COMT using the molecule mechanics/Poisson–Boltzmann surface area (MM/PBSA) method in AMBER 11. The binding free energy was calculated as the difference of the free energy of each molecule species (complex, protein, and ligand):

$$\Delta G_{\text{bind}} = G_{\text{complex}} - (G_{\text{protein}} + G_{\text{ligand}}) = \Delta E_{\text{MM}} + \Delta G_{\text{sol}} - T\Delta S \quad (1)$$

where ΔE_{MM} is the molecule mechanics energy, which consists of the electrostatic and van der Waals interactions and the internal energy term (bond, angle, and dihedral energies):

$$\Delta E_{\text{MM}} = \Delta E_{\text{ele}} + \Delta E_{\text{vdw}} + E_{\text{internal}} \quad (2)$$

in which $\Delta E_{\text{internal}}$ is omitted in the MD calculation, since there is no covalent bond formed between flavonoid and COMT.

ΔG_{sol} was the solvation free energy, which was composed of the polar and nonpolar contribution:

$$\Delta G_{\text{sol}} = \Delta G_{\text{ele,sol}} + \Delta G_{\text{nonpol,sol}} \quad (3)$$

$\Delta G_{\text{ele,sol}}$ could be obtained by solving the Poisson–Boltzmann (PB) equation[45] in the MM-PBSA method. The nonpolar solvation contribution $\Delta G_{\text{nonpol,sol}}$ was determined from the solvent accessible surface area (SASA, Å^2) as shown below:

$$\Delta G_{\text{nonpol,sol}} = \gamma \text{SASA} + \beta \quad (4)$$

The surface tension parameter γ and the offset value were default set to be 5.42×10^{-3} kcal/mol·Å^2 and −1.008, respectively.

The conformational entropy term (translation, rotation, and vibration) in eq 1 was obtained by using the NMODE[46] module after a minimization for 100 000 steps with a distance-dependent dielectric constant, $\varepsilon = 4r$, until the root mean square of the elements of the gradient vector was less than 1.0×10^{-3} kcal/mol·Å^2. In consideration of the high computational demand of this approach, only 40 snapshots taken from the MD trajectory of the last 2 ns at 50 ps intervals were utilized to estimate the entropic contribution.

Per-Residue Free Energy Decomposition Analyses. In order to provide insight into the changes that occur in the energetic profile of COMT–flavonoid interaction over the course of the trajectory, the binding free energies were further decomposed to each residue's contribution to ligand using the MM/PBSA[25] module in AMBER 11. By compared to total binding free energy calculations, the per-residue free energy decomposition could reveal each residue's impact on ligand, which will allow us to analyze more deeply and clearly the binding capability and selectivity of each inhibitor. It can be calculated according to the equation

$$\Delta G_{\text{inhibitor-residue}} = \Delta E_{\text{vdW}} + \Delta E_{\text{ele}} + \Delta G_{\text{ele,sol}} + \Delta G_{\text{nonpol,sol}} \quad (5)$$

In the above equation, ΔE_{vdW} and ΔE_{ele} are van der Waals and electrostatic interactions. The polar contribution of solvation ($\Delta G_{\text{ele,sol}}$) was calculated using the generalized Born (GB) model with the parameters developed by Onufriev et al.[47] The nonpolar contribution of solvation ($\Delta G_{\text{nonpol,sol}}$) was computed on the basis of SASA determined with the ICOSA method.[25] The same snapshots utilized in binding free energy calculations were used.

QM Calculations on the Flavonoids. To investigate the chemical reactivity difference of 3′-OH and 4′-OH in each conformation of luteolin and quercetin, we also calculated the atomic charges derived from natural population analysis (NPA)

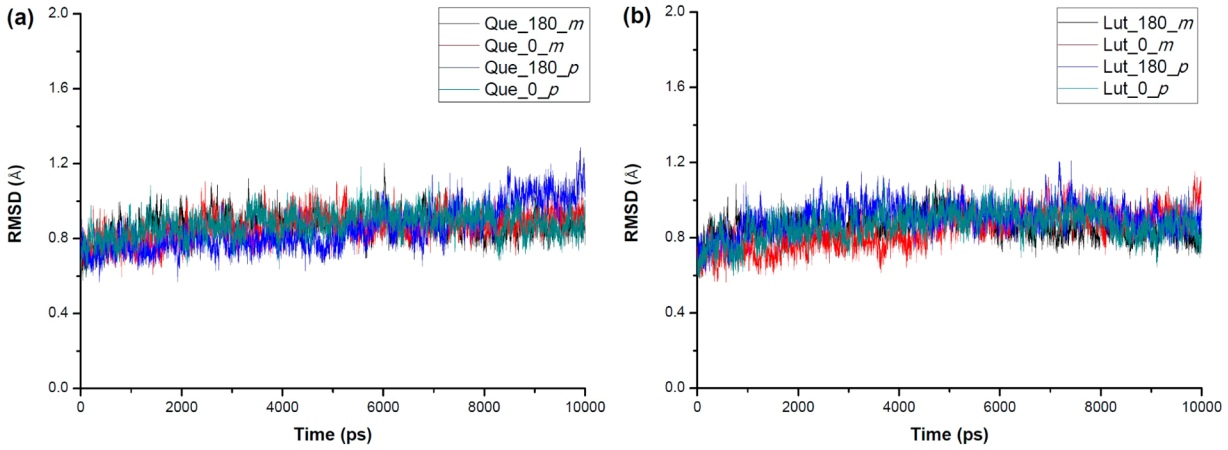

Figure 3. RMSDs of backbone atoms of (a) COMT-AdoMet-quercetin systems and (b) COMT-AdoMet-luteolin systems as a function of the simulation time.

using different methods (B3LYP, B3PW91, M06-2X) with the 6-311++G(d,p) basis set based on the corresponding structures optimized by the same level of theory. To account for solvation effects, we employed the integral equation formalism polarizable continuum model (IEFPCM) with water as solvent. All the QM calculations were performed using the Gaussian 09 program.

QM/MM Calculations on the Complexes. Four MD-simulated complexes, which were suggested to have energetically stable either quercetin or luteolin binding to COMT for their *para*-O-methylations or *meta*-O-methylations by MM/PBSA binding free energy computations, were chosen to do QM/MM calculations of reaction energy barriers. The initial structure for the QM/MM calculation of each reactant complex was based on the representative snapshot taken from the last 2 ns of the MD trajectory. Since the catalytic efficacy of the enzyme was demonstrated to be influenced by how often the nucleophile and electrophile are positioned in near attack conformations (NACs),[48] a conformational criterion was applied for the selection of the starting snapshots to reduce the artificial bias, making the results of the QM/MM calculations in each complex more comparable. The distance $d(C\cdots O_M)$ between the catechol-O_M, which means the oxygen atom to be methylated in flavonoid, and the S−CH_3 carbon of AdoMet was required to be in the range from 2.95 to 3.15 Å, and the corresponding S−C···O_M angle $A(SCO_M)$ was limited in the range from 160 to 170°. Both $d(C\cdots O_M)$ and $A(SCO_M)$ were also required to be within the range of average ± std dev (standard deviation) of the last 2 ns MD simulations. As for each of the selected snapshots, water molecules that are only within 5 Å of protein or 12 Å of the flavonoid were kept, while all other water molecules were erased to reduce the computational cost, thus resulting in approximately 7660 atoms in the whole system. The four simplified solvation systems were subjected to subsequent geometry optimization following the same three steps as described in the MD Simulations section to eliminate some improper distortions and, more importantly, diminish the bias toward any binding mode in the selection of starting geometries.

In our investigation of the reaction process in each complex by QM/MM calculations, no structural constraint was applied for the sake of gaining insights into the system more realistically. A two-layer ONIOM method[49−52] in Gaussian 09 was implemented for all QM/MM calculations. As illustrated in Figure 2, Mg^{2+}, AdoMet, flavonoid, the water molecule coordinated to Mg^{2+}, and part of COMT's residues Asp141, His142, Trp143, Lys144, Asp169, Asn170, and Glu199 (92 and 93 atoms, respectively, when the ligand is luteolin or quercetin) were included in the QM region, while the remainder of the entire system was treated as the MM part. It should be noted that, in our initial QM/MM model, the catechol moiety of the flavonoid was altered to the neutral form while Glu199 and Lys144 were set to be deprotonated to examine the prototropic performance. Optimized stationary points including reactants, intermediates, transition states, and products were obtained at the B3LYP/6-31G(d,p) level of theory for the QM layer, and the AMBER96 force field for the MM layer. Electrostatic interactions between QM and MM regions were treated using the mechanical embedding (ME) scheme. To ensure the validity of the transition states, frequency calculations were performed at the same level of theory as the optimization step. The QM/MM frequency calculations included atoms in the QM layer and MM region around 5 Å of the core residues Asp141, His142, Trp143, Lys144, Asp169, Asn170, Glu199, Mg^{2+}, AdoMet, flavonoid, and the water molecule coordinated to Mg^{2+}. Refined structures were finally subjected to single point energy calculations at the ONIOM(B3LYP/6-311++G(d,p):AMBER) level of theory based on mechanical embedding.

RESULTS AND DISCUSSION

MD Simulations of Eight Complexes of COMT-AdoMet-Flavonoid-Mg^{2+}. Molecule dynamics computations were carried out on the complexes of COMT-AdoMet-luteolin-Mg^{2+} or COMT-AdoMet-quercetin-Mg^{2+} in explicit aqueous solution for 10 ns to simulate the stable binding modes of luteolin or quercetin for the corresponding *para*-methylation or *meta*-methylation catalyzed by COMT. MD-simulated structural models of COMT-AdoMeT-luteolin-Mg^{2+} or COMT-AdoMet-quercetin-Mg^{2+} were also used as the initial structures for later QM/MM studies. As shown in Figure 3, root-mean-square deviations (RMSDs) from the starting structure were analyzed to ensure the stability of each system. It can be seen from the plots that each complex achieved equilibrium after 2−3 ns rapidly, with the backbone of protein fluctuating at around 1.0 Å. Such small fluctuations indicated the rationality of our simulations and the trajectories obtained. The representative

dx.doi.org/10.1021/jp410296s | J. Phys. Chem. B 2014, 118, 470−481

Table 2. Structural Parameters in the Reaction Center

	distance (Å)			angle (deg)
system	$d(C\cdots O_M)^a$	$d(Mg^{2+}\cdots O_M)^b$	$d(Mg^{2+}\cdots O)^c$	$A(SCO_M)^d$
Que_180_*m*	3.02 ± 0.13	1.92 ± 0.05	2.04 ± 0.08	166.3 ± 6.3
Que_0_*m*	2.97 ± 0.12	1.91 ± 0.05	2.08 ± 0.10	164.2 ± 6.6
Que_180_*p*	3.00 ± 0.13	2.00 ± 0.07	1.98 ± 0.07	161.3 ± 7.0
Que_0_*p*	3.05 ± 0.14	1.99 ± 0.07	1.96 ± 0.07	161.3 ± 7.2
Lut_180_*m*	3.05 ± 0.15	1.91 ± 0.05	2.05 ± 0.09	162.8 ± 7.9
Lut_0_*m*	3.09 ± 0.15	1.90 ± 0.05	2.00 ± 0.07	166.7 ± 6.4
Lut_180_*p*	3.10 ± 0.15	1.98 ± 0.07	1.96 ± 0.06	158.8 ± 7.5
Lut_0_*p*	3.03 ± 0.13	1.97 ± 0.06	1.98 ± 0.07	161.4 ± 7.0

[a]The distance between the carbon atom of the S−CH_3 group of AdoMet and the oxygen atom O_M to be methylated on the catechol moiety of flavonoid. [b]The distance between Mg^{2+} and the oxygen atom O_M to be methylated on the catechol moiety of flavonoid. [c]The distance between Mg^{2+} and another oxygen atom O relative to O_M on the catechol moiety. [d]The angle among three atom S−C···O_M.

Table 3. Gaussian-Computed NPA Charges (ev) of *meta*-O and *para*-O in Luteolin and Quercetin

	B3LYP		B3PW91		M06-2X	
flavonoids	*meta*-O	*para*-O	*meta*-O	*para*-O	*meta*-O	*para*-O
Que_180	−0.685	−0.676	−0.678	−0.669	−0.696	−0.690
Que_0	−0.687	−0.677	−0.679	−0.669	−0.697	−0.690
Lut_180	−0.683	−0.674	−0.676	−0.666	−0.694	−0.688
Lut_0	−0.683	−0.673	−0.676	−0.665	−0.694	−0.687

Table 4. MM/PBSA Binding Free Energies and Energy Components (kcal/mol)

system	ΔE_{vdw}	ΔE_{ele}	$\Delta G_{ele,sol}$	$\Delta G_{ele} + \Delta G_{ele,sol}$	$\Delta G_{nonpol,sol}$	$T\Delta S$	ΔG_{bind}
Que_180_*m*	−8.50 ± 4.44	−246.19 ± 14.60	178.06 ± 11.53	−68.13	−1.48 ± 0.13	−16.87 ± 2.55	−61.24
Que_0_*m*	−7.59 ± 4.19	−250.14 ± 14.75	174.17 ± 12.23	−75.97	−1.31 ± 0.09	−16.28 ± 5.01	−68.59
Que_180_*p*	−10.71 ± 4.21	−252.66 ± 16.60	181.94 ± 14.58	−70.72	−1.63 ± 0.09	−16.07 ± 4.29	−66.99
Que_0_*p*	−6.99 ± 4.09	−261.97 ± 14.09	192.59 ± 11.43	−69.38	−1.27 ± 0.10	−17.33 ± 4.62	−60.31
Lut_180_*m*	−6.71 ± 4.12	−273.94 ± 14.07	196.70 ± 11.56	−77.24	−1.70 ± 0.10	−15.85 ± 3.37	−69.80
Lut_0_*m*	−5.47 ± 3.94	−249.11 ± 13.10	181.19 ± 10.75	−67.92	−1.21 ± 0.11	−15.94 ± 3.68	−58.66
Lut_180_*p*	−9.52 ± 4.63	−270.72 ± 15.35	190.06 ± 11.70	−80.66	−1.70 ± 0.08	−19.01 ± 3.43	−72.87
Lut_0_*p*	−6.79 ± 4.19	−263.66 ± 15.38	187.39 ± 15.69	−76.27	−1.27 ± 0.10	−16.56 ± 6.60	−67.77

models of eight MD-simulated complexes were illustrated in Figure S4 in the Supporting Information.

Table 2 lists some important structural parameters of the reaction center obtained from the last 5 ns of MD. For both luteolin and quercetin binding to COMT integrating AdoMet and Mg^{2+}, the average distance $d(C\cdots O_M)$ between the carbon atom of the S−CH_3 group in AdoMet and the pre-methylated oxygen atom of flavonoids lies in the narrow range of 2.95−3.10 Å in each system. Furthermore, in the case of the corresponding angle $A(SCO_M)$, the pre-methylated *meta*-O is a little more linear with the carbon atom of the methyl group and the sulfate atom as compared to *para*-O pointing to AdoMet's S−CH_3 group to be ready for its methylation (e.g., 164.2° in QUE_180_*m* versus 161.3° in QUE_180_*p* and 162.8° in Lut_0_*m* versus 158.8° in Lut_0_*p*). Such a linear conformation would be beneficial to the S_N2 attack of the catecholic oxygen to the methyl group bonded on the sulfate atom of AdoMet, which would be further confirmed by the QM/MM-computed transition state.

As indicated in Table 2, the oxygen atoms in the catecholic hydroxyl group are ligated to the Mg^{2+} rigidly with average distances of 1.90−2.10 Å. For the complexes Que_180_*m*, Que_0_*m*, Lut_180_*m*, and Lut_0_*m*, in which the 3′-O atom of luteolin or quercetin was set for methylation, the distance $d(Mg^{2+}\cdots O_M)$ between 3′-O and Mg^{2+} is shorter than the distance $d(Mg^{2+}\cdots O)$ between 4′-O and Mg^{2+}. As for the other four complexes Que_180_*p*, Que_0_*p*, Lut_180_*p*, and Lut_0_*p*, the distance $d(Mg^{2+}\cdots O_M)$ between 4′-O and Mg^{2+} is almost the same as the distance $d(Mg^{2+}\cdots O)$ between 3′-O and Mg^{2+}. Overall, the pre-methylated *meta*-O atom of luteolin or quercetin is slightly more tightly coordinated to the metal center than their pre-methylated *para*-O atom. In fact, the RESP charges of the *meta*-O and *para*-O are about $-0.7e^-$ and $-0.8e^-$, respectively, for both luteolin and quercetin, so it is clear that the more negative charge contributes to the binding stability with Mg^{2+}. Compared to luteolin, quercetin has an additional 3-OH group, which would be electron-donating in quercetin with a delocalized π bond. Therefore, *ab initio* calculations were performed on a single molecule of either luteolin or quercetin to see whether such an additional hydroxyl group would induce different atomic charge distributions on two oxygen atoms in catechol moieties of luteolin and quercetin.

QM Calculations on the Charge Distribution of Flavonoids. In order to confirm that the 3′-O atom bears more negative charge than the 4′-O atom of both luteolin and quercetin, we carried out *ab initio* calculations on these two flavonoids. Table 3 showed the partial charges of *meta*-O and *para*-O in luteolin and quercetin calculated by different methods. As indicated in all *ab initio* computations, either luteolin or quercetin has more negative charge on the *meta*-O atom than the *para*-O atom. These results indicated that *meta*-

dx.doi.org/10.1021/jp410296s | J. Phys. Chem. B 2014, 118, 470−481

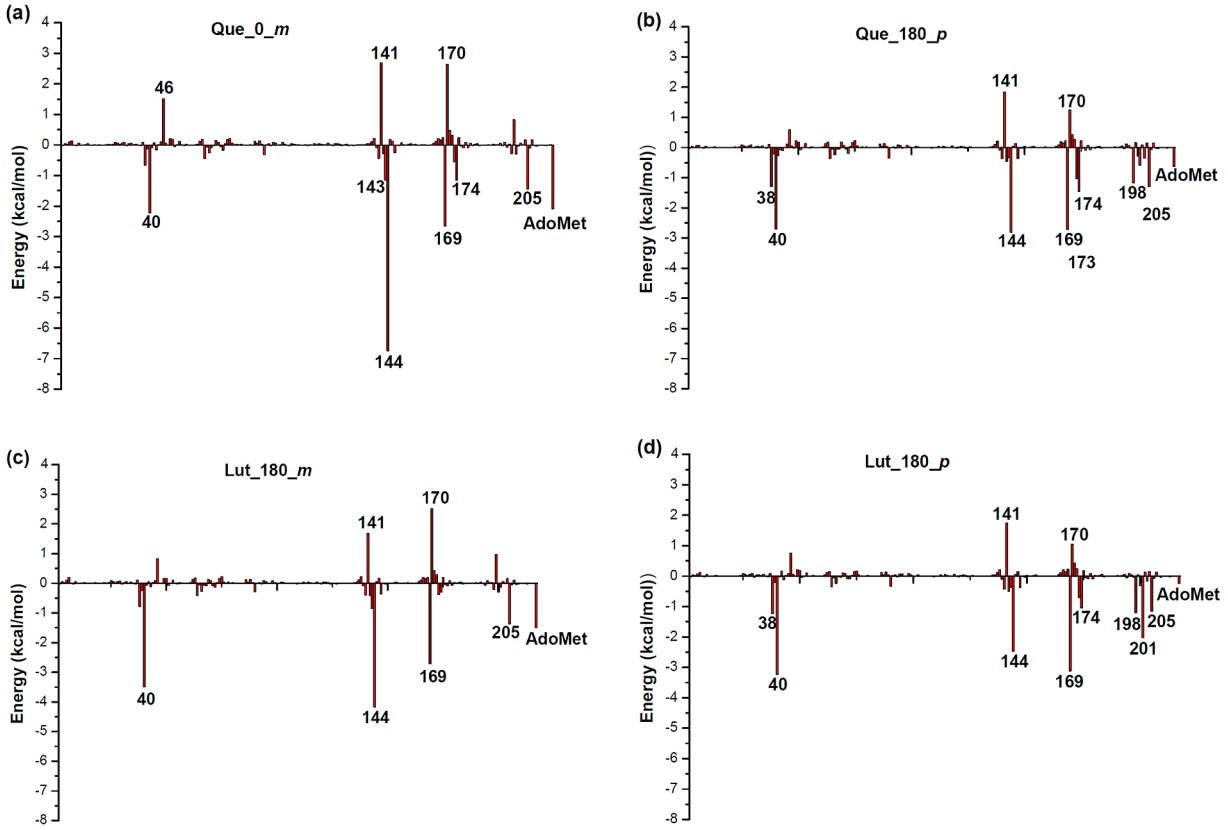

Figure 4. Per-residue energy decomposition of (a) Que_0_*m*, (b) Que_180_*p*, (c) Lut_180_*m*, and (d) Lut_180_*p*.

O atoms of both luteolin and quercetin would be more nucleophilic than their *para*-O atoms. On the basis of general knowledge about the S_N2 reaction, our quantum chemical calculations displayed that *meta*-OH would have a higher reaction capability for its methylation than the *para*-OH group. However, our experimental data indicated that quercetin has more *meta*-O methylation than *para*-O methylation but luteolin has more *para*-O methylation than *meta*-O methylation. As discussed later, it would be confirmed whether *meta*-O atoms of both luteolin and quercetin were more easily methylated than their *para*-OH groups in the enzymatic environment by performing QM/MM calculations. Before that, we did binding free energy calculations on the basis of eight MD-simulated structural models of quercetin and luteolin, respectively, binding to COMT.

Binding Free Energy Analyses. Table 4 lists the calculated binding free energies and their components of each conformation of both quercetin and luteolin, respectively, binding to COMT for *meta*-O methylation or *para*-O methylation using the MM/PBSA method. The resulting balance of the favorable Coulombic interactions between flavonoids and COMT with AdoMet and Mg^{2+} and the unfavorable electrostatics of desolvation ($\Delta G_{ele} + \Delta G_{ele,sol}$) is to the benefit of binding in all eight systems with a contribution of approximately −65 to −80 kcal/mol to the binding free energy. The hydrophobic interactions, including the van der Waals interactions (ΔG_{vdw}: −5 to −11 kcal/mol) and the nonpolar solvation energies ($\Delta G_{nonpol,sol}$: −1 to −2 kcal/mol) responsible for the burial of the ligand's hydrophobic groups, play a much lesser role in the binding stability of quercetin or luteolin. This observation is likely due to the strong Coulombic interactions between catechol-O^- and Mg^{2+}, or it is the fact that the binding pocket is located on the surface of COMT to let the flavonoid be partly exposed to the solvent.

As we knew, either quercetin or luteolin has two conformations, with the dihedral angle Φ(C3−C2−C1′−C2′) values of near 180 or 0°, respectively, binding to different proteins.[30−33] The dihedral angle Φ(C3−C2−C1′−C2′) between rings B and C could either be near 0 or 180°, which was supported by a high level of density functional computations. Actually, Monica et al.[24] reported that quercetin's energy expenditure of reciprocal transformation from Φ = 0° to Φ = 180° was theoretically estimated to be only about 2.4 kcal/mol. Our further computations indicated that luteolin has a corresponding energy of about 4.2 kcal/mol for reciprocal transformation from Φ = 0° to Φ = 180° (Figure S5 in the Supporting Information). Therefore, all of these two conformations of quercetin or luteolin could be possibly binding to COMT for their *meta*-O methylation or *para*-O methylation. By comparing the calculated binding free energies, it can be proposed which conformation would be preferable for each compound binding to COMT for their *meta*-O methylation or *para*-O methylation. As indicated in Table 4, the conformation Que_180 has −7.35 kcal/mol lower binding free energy (ΔG_{bind}) than the conformation Que_0 for *meta*-O methylation of quercetin. In contrast, Que_0 has −6.68 kcal/mol lower binding free energy than Que_180 for *para*-O methylation of quercetin. Therefore, it could be suggested that quercetin would take the conformation Que_180 for its *meta*-O methylation and the conformation Que_0 for its *para*-O methylation. In addition, the calculated binding free energy is −68.59 kcal/mol in system Que_0_*m* but −66.99 kcal/mol in system Que_180_*p*, which means quercetin has a more stable binding mode (Que_0_*m*) for its *meta*-O methylation than that

dx.doi.org/10.1021/jp410296s | J. Phys. Chem. B 2014, 118, 470−481

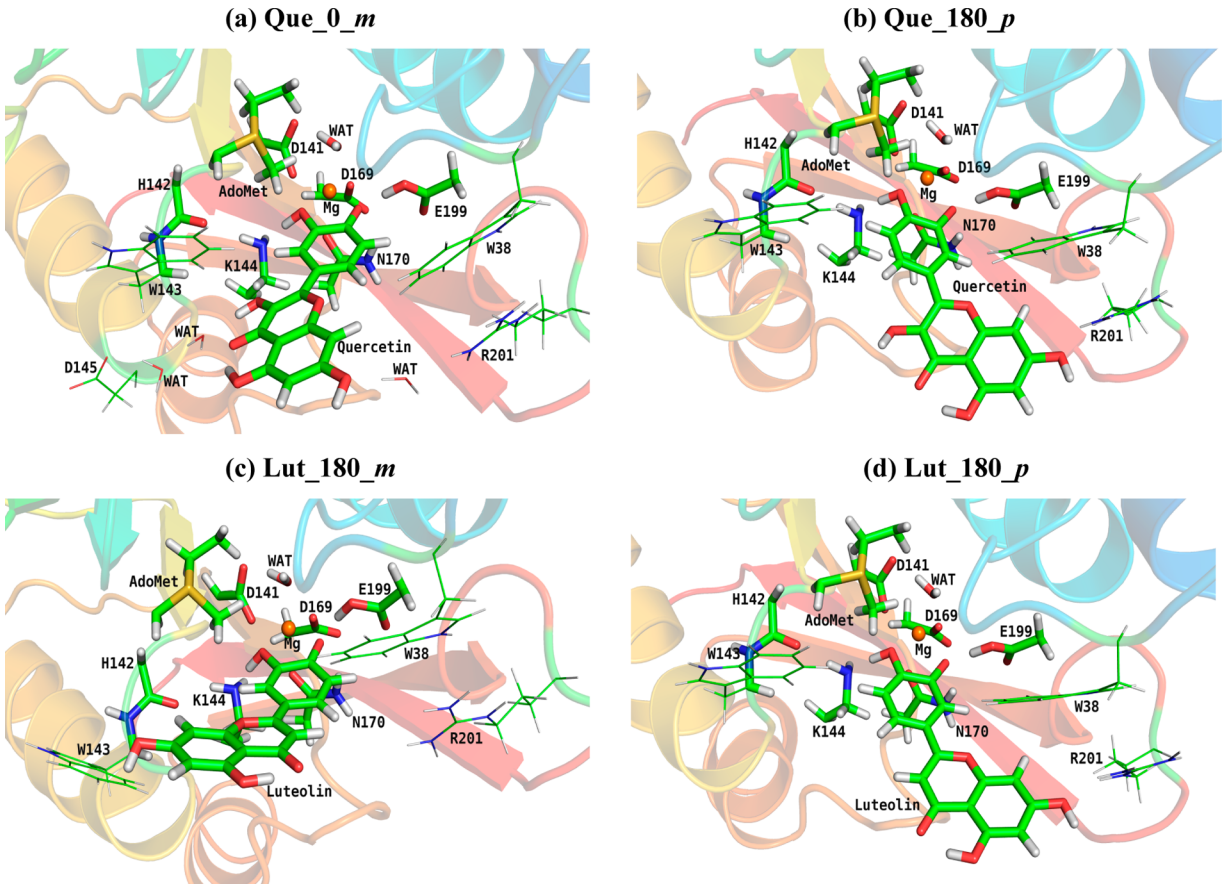

Figure 5. Optimized structures of four complexes: (a) Que_0_*m*, (b) Que_180_*p*, (c) Lut_180_*m*, and (d) Lut_180_*p* by the QM/MM method. Atoms shown in sticks and spheres (Mg^{2+}) are included in the QM region.

(Que_180_*p*) for its *para*-O methylation. As for the compound luteolin, the conformation Lut_180 has −11.14 kcal/mol lower binding free energy (ΔG_{bind}) than the conformation Lut_0 for *meta*-O methylation of luteolin. In the meantime, Lut_180 has −5.10 kcal/mol lower binding free energy than Lut_0 for *para*-O methylation of luteolin. Therefore, it could be suggested that luteolin would take the same conformation Lut_180 for its *meta*-O methylation and *para*-O methylation. In addition, the calculated binding free energy is −69.80 kcal/mol in system Lut_180_*m* but −72.87 kcal/mol in system Lut_180_*p*, which means that luteolin has a more stable binding mode (Lut_180_*m*) for its *para*-O methylation than that (Lut_180_*p*) for its *meta*-O methylation. Above all, it can be hypothesized that the two flavonoids quercetin and luteolin have differently preferable binding modes for their *meta*-O methylation and *para*-O methylation. The results of the binding free energy calculations are congruent with the experimental data. As illustrated in Figure S4 in the Supporting Information for eight MD-simulated systems, four structural models, Que_0_*m*, Que_180_*p*, Lut_180_*m*, and Lut_180_*p*, were chosen to do QM/MM calculations for their reaction energy barriers.

Analyses of Interaction Modes of Flavonoids Binding to COMT. The per-residue binding free energy decomposition was further conducted to reveal intermolecular interactions between each flavonoid and the key residues around the binding pocket of COMT on the basis of MD-simulated structural models of four systems, Que_0_*m*, Que_180_*p*, Lut_180_*p*, and Lut_180_*p*, since these four systems have lower binding free energies for the *para*-O methylations or *meta*-O methylations of quercetin and luteolin. As shown in Figure 4, the residues Met40, Lys144, Asp169, and Asp205 provide major favorable interactions with flavonoids in all four systems, but Asp141 and Asn170 bear unfavorable energy contributions in common. In addition, Mg^{2+} has very strong electronic interactions with quercetin or luteolin by energy contributions of −36.00, −34.00, −33.92, and −35.05 kcal/mol, respectively, in the above four systems, to each flavonoid's binding in the active pocket of COMT owing to the strong coordination between Mg^{2+} and the catecholic oxygen atoms, As discussed in the previous section, Que_0_*m* bears a more favorable binding mode in comparison to Que_180_*p*. The per-residue binding free energy decomposition indicated that the COMT's residues Trp143 and Lys144, Adomet and Mg^{2+}, are mainly responsible for the differences. The energetic contribution of the hydrophobic residue Trp143 is −0.33 kcal/mol in Que_180_*p* but −1.15 kcal/mol in Que_0_*m*. In contrast, the hydrophilic residue Lys144 contributes −6.74 kcal/mol in Que_0_*m* but only −2.80 kcal/mol in Que_180_*p*, indicating that the *meta*-O of quercetin has a more favorable electrostatic interaction with Lys144 as compared to the *para*-O. The positively charged AdoMet and Mg^{2+} could accept quercetin more comfortably and stably in the case of Que_0_*m* (−38.09 kcal/mol) rather than Que_180_*p* (−34.63 kcal/mol). These results matched the previous atomic charge distribution computations which displayed the *meta*-O atom of quercetin has more negative atomic charge than its *para*-O atom. As for luteolin, its *para* binding mode (Lut_180_*p*) was estimated to

dx.doi.org/10.1021/jp410296s | J. Phys. Chem. B 2014, 118, 470−481

be preferable to its binding mode (Lut_180_*m*) for the *meta*-O methylation. Such an adverse phenomenon could be partly attributed to the more favorable contribution of van der Waals interaction of the residues Trp38, Pro174, Leu198, and Arg201 of COMT to Lut_180_*p* compared with Lut_180_*m*. Regarding the contribution of the positive center formed by Mg^{2+} and AdoMet, the gap between *para*-O and *meta*-O binding modes is narrowed down from 3.46 kcal/mol (quercetin) to 1.86 kcal/mol (luteolin), which may be caused by the absence of the electronegative and hydrophilic 3-OH.

QM/MM Investigation on the Reversed Regioselectivity. As discussed in the previous sections, MD simulations and binding free energy calculations have suggested four preferred structural models of luteolin or quercetin binding to COMT for their *meta*-O methylation and *para*-O methylation, respectively. These four MD-simulated complexes were further applied to investigate the reaction energy barriers of COMT-catalyzed methylations by QM/MM calculations of reactants' states, transition states, and products' states. Figure 5 illustrated QM/MM optimized structures of the four selected complexes from the MD simulations. According to our ONIOM calculations, the distance $d(C\cdots O_M)$ and angle $A(SCO_M)$ of each complex distribute rigidly at the range of 2.68−2.74 Å and 172.0−176.0°, respectively. These are in agreement with the crystal structure (pdb entry: 3BWY), in which the catechol moiety of 3,5-dinitrocatechol binds to the active site of COMT with a distance $d(C\cdots O_M)$ of 2.72 Å and angle $A(SCO_M)$ of 173.9°. As mentioned above, the flavonoid was originally set to a neutralized form in the QM/MM studies. Intriguingly, the catechol-OH hydroxyl proton initially forming a hydrogen bond with the carboxyl group of Glu199 transferred automatically to Glu199 in all systems during the QM/MM optimization. In fact, our energetic scanning calculations indicated that it is an energy-favorable process for proton to transfer from the catecholic hydroxyl group of flavonoid to the carboxyl group of Glu199 (Figure S3 in the Supporting Information). This could be mainly attributed to the decrease of pK_a of the catechol moiety. In addition, the hydrogen bond formed between the catechol oxygen atom and the amide side chain of Asn170 is also propitious to the stabilization of the ionized catechol-O atom (Figure 5).

On the other hand, some significant differences could be observed. As shown in Figure 5, the rings A, B, and C of quercetin in Que_0_*m* stay closely with Trp143 and Trp38 to form favorable hydrophobic interactions. Trp143 separates from quercetin in the case of Que_180_*p*. It was found that the 7-OH of quercetin is hydrogen bonded directly to Arg201 in Que_180_*p*, while as for Que_0_*m*, this hydrogen bond is mediated by a water molecule. Moreover, a two water molecule mediated hydrogen bond could also be found between Asp145 and the 3-OH of quercetin in Que_0_*m*. It is noted that these differences in substrate−enzyme interactions may be overall more favorable for Que_0_*m*. As for luteolin, the corresponding water molecules mediated hydrogen bonds do not exist in Lut_180_*m*, serving as a positive factor contributing to the regioselectivity toward *para*-O methylation of luteolin.

To further examine the relationship between kinetic characters and the methylation selectivity, we performed reaction barrier calculations. The structures of reactants in each complex are illustrated in Figure 5, and the corresponding structures of translation states were displayed in Figure S6 in the Supporting Information. The QM/MM energy profiles were obtained on the basis of the ONIOM-EE (B3LYP/6-311+G(d,p):AMBER) single point energy calculation. As shown in Figure 6, the processes of COMT-catalyzed methylations were

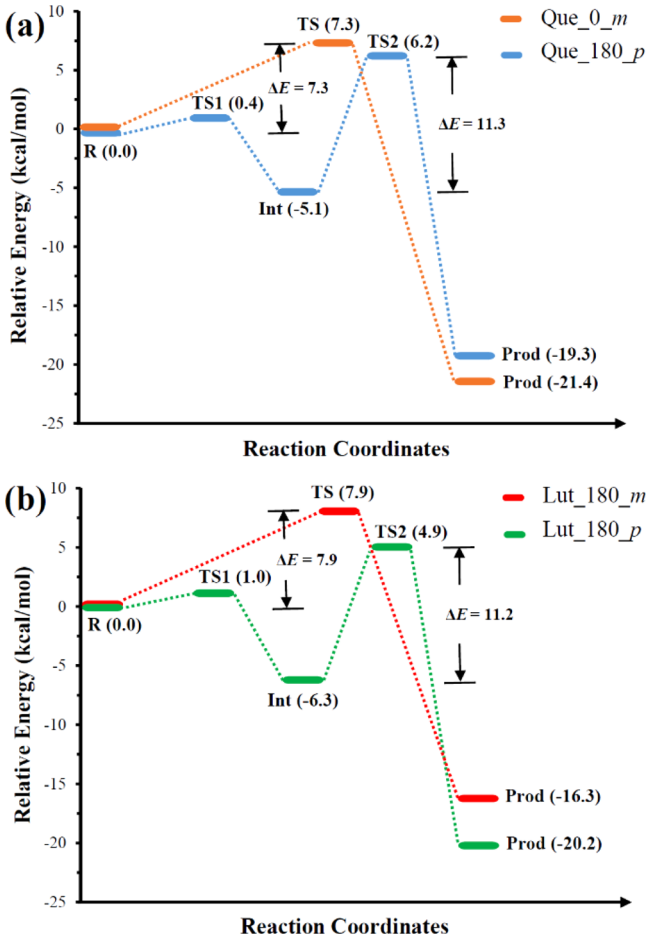

Figure 6. Reaction energy profiles of (a) quercetin and (b) luteolin methylations catalyzed by human COMT. Energies were obtained at the B3LYP/6-311++G**//B3LYP/6-31G** level.

calculated to be a two-step S_N2 displacement reaction in the cases of Que_180_*p* and Lut_180_*p* for the *para*-O-methylations of quercetin and luteolin. In Que_180_*p* and Lut_180_*p*, the reaction begins with proton transfer from the pre-methylated catechol-OH group to the amino group of Lys144, and then the ionized catechol-O^- attacks the methyl group of AdoMet to yield the methylation product. The latter is the rate-limiting step, with a much higher reaction barrier. On the other hand, the COMT-catalytic processes were calculated to be a concerted S_N2 displacement reaction in the cases of Que_0_*m* and Lut_180_*m* for their *meta*-O-methylations. Such a phenomenon was supported by our energy scanning calculations for the proton transfer from the pre-methylated OH group of either quercetin or luteolin to the residue Lys144 of COMT. As illustrated in Figure S7 in the Supporting Information, the proton transfer from the *meta*-catechol-OH group to the amino group of Lys144 was an energetic raising process in the system of Que_0_*m* or Lut_180_*m* for the *meta*-O methylations of quercetin and luteolin, but the proton transfer from the *para*-OH group to the amino group of Lys144 had an energy barrier, which was calculated to be the first transition state (Figure S6b or S6e in the Supporting Information), in the system of Que_180_*p* or Lut_180_*p* for

dx.doi.org/10.1021/jp410296s | J. Phys. Chem. B 2014, 118, 470−481

their *para*-O methylations. That is probably because the corresponding hydrogen on *meta*-OH is more attracted by the oxygen atom than that on *para*-OH, since our previous *ab initio* calculations indicated that the 3′-O atom had a more negative charge than the 4′-O atom in either quercetin or luteolin.

As illustrated in Figure 6, the energy barrier of the *meta*-O-methylation reaction of quercetin (ΔE = 7.3 kcal/mol) is 4.0 kcal/mol lower than that of its *para*-O-methylation (ΔE = 11.3 kcal/mol in the second step). Both methylations are exothermic reactions, while the former is 7.2 kcal/mol more exothermic. Luteolin has corresponding energy barriers estimated to be 7.9 kal/mol for its *meta*-O-methylation and 11.2 kcal/mol in the rate-limiting step of its *para*-O-methylation, with a disparity of 3.3 kcal/mol. Similar to quercetin, both *meta*-O and *para*-O methylations of luteolin are exothermic, while the gap now narrows to 2.4 kcal/mol, but is still advantageous to *meta*-O-methylation. As a result, our QM/MM calculations of COMT-catalyzed methylations indicated that both quercetin and luteolin have lower reaction energetic barriers for *meta*-O-methylation than *para*-O-methylation. It is believed that both quercetin and luteolin are kinetically more favorable to be methylated at *meta*-O by human COMT. Combined with the results from *ab initio* calculations of atomic charge distributions, it could be assumed that the 3-OH group in quercetin does not influence the nucleophilic reaction capabilities of the two phenyl hydroxyl group on its catecholic moiety. On the other hand, our MM/PBSA calculations have shown that luteolin has a lower binding free energy with COMT for its *meta*-O-methylation but quercetin has a lower binding free energy with the conformation for the *para*-O-methylation. As demonstrated by our experimental data, luteolin has preferred *meta*-O-methylation catalyzed by COMT but quercetin has preferred *para*-O-methylation. Therefore, it could be hypothesized that the stable interaction mode of flavonoid binding to COMT would be a key factor to control the regioselectivity of COMT-promoted methylation. This phenomenon may result from the higher nucleophilicity of 3′-O caused by the electron-withdrawing effect of aromatic A and C rings. Moreover, the barrier gap and exothermic energy gap between *meta*-O-methylation and *para*-O-methylation lie smaller in the case of luteolin, indicating that the kinetics tendency of methylation on *meta*-O is weaker in luteolin than quercetin. This is likely due to the electron conjugated effect of 3-OH in quercetin which may partially counteract the electron-withdrawing effect of A−C rings.

CONCLUSIONS

The COMT-promoted O-methylation regioselectivity of quercetin or luteolin was investigated using the MD simulations, binding free energy calculations, and QM/MM studies. For both quercetin and luteolin, the MD analyses reveal that, when the flavonoid points its *meta*-O to the methyl group of AdoMet, the average angle $A(SCO_M)$ is larger, thus resulting in more *meta*-O-methylation products. This factor contributes to the regioselectivity of 3′-O-methylation and we classify it to the kinetics category. However, the binding free energy calculations and QM/MM optimization show that the *meta*-O-methylation binding mode of quercetin and *para*-O-methylation binding mode of luteolin respectively possess the more favorable interactions with the active site of human COMT. It is clear that this factor belonging to the thermodynamics category contributes to the regioselectivity of *meta*-O-methylation of quercetin and, more notably, the regioselectivity of *para*-O-methylation of luteolin. According to the QM/MM calculations of the reaction process, regarding both quercetin and luteolin, the barrier heights lie lower in the case of *meta*-O-methylation than *para*-O-methylation while the exothermic energy lies greater in the corresponding cases. Meanwhile, this kinetics gap was predicted to be narrower when the substrate is luteolin. Hence, we came to the conclusion that the methylation regioselectivities of quercetin and luteolin are comprehensive results jointly induced by both kinetics and thermodynamics. For quercetin, both of the two are in favor of *meta*-O-methylation. However, for luteolin, the kinetics factors go against the regioselectivity, while thermodynamics is in favor and actually dominating. This is also in accordance with the higher selectivity for *meta*-O-methylation in quercetin (about 3.0) than in luteolin (about 0.7).

ASSOCIATED CONTENT

Supporting Information

Material and methods, results (Figure S1) of COMT-catalyzed *meta*-/*para*-methylations of quercetin and luteolin, the structural diagrams of other six complexes, Que_180_*m*, Que_0_*p*, Lut_180_*m*, Lut_0_*m*, Lut_180_*p*, and Lut_0_*p* (Figure S2), the energetic scanning calculations of proton transfer from catecholic hydroxyl group to carboxyl group of COMT's Glu199 (Figure S3), the MD-simulated structure model of eight systems (Figure S4), computations of rotation energy barrier of luteolin for reciprocal transformation from Φ (C3−C2−C1′−C2′) = 0° to Φ (C3−C2−C1′−C2′) = 180°(Figure S5), the energetic scanning calculations of proton transfer from pre-methylated catecholic hydroxyl group to the amino group of COMT's Lys144 (Figure S6), transition states for the COMT-catalyzed *meta*-/*para*-O methylations of both quercetin and luteolin (Figure S7). This material is available free of charge via the Internet at http://pubs.acs.org.

AUTHOR INFORMATION

Corresponding Author

*E-mail: chjz@zju.edu.cn. Phone and fax: 86-571-88208659.

Notes

The authors declare no competing financial interest.

ACKNOWLEDGMENTS

The National Science Foundation of China (Grant No. 81172983 and 81302840) is gratefully acknowledged for financial support.

REFERENCES

(1) Guldberg, H. C.; Marsden, C. A. Catechol-O-Methyltransferase: Pharmacological Aspects and Physiological Role. *Pharmacol. Rev.* **1975**, *27*, 135−246.

(2) Tenhunen, J.; Salminen, M.; Lundström, K.; Kiviluoto, T.; Savolainen, R.; Ulmanen, I. Genomic Organization of the Human Catechol O-methyltransferase Gene and Its Expression from Two Distinct Promoters. *Eur. J. Biochem.* **1994**, *223*, 1049−1059.

(3) Tai, C.-H.; Wu, R.-M. Catechol-O-methyltransferase and Parkinson's Disease. *Acta Med. Okayama* **2002**, *56*, 1−6.

(4) Palma, P. N.; Rodrigues, M. L.; Archer, M.; Bonifacio, M. J.; Loureiro, A. I.; Learmonth, D. A.; Carrondo, M. A.; Soares-da-Silva, P. Comparative Study of Ortho- and Meta-nitrated Inhibitors of Catechol-O-methyltransferase: Interactions with the Active Site and Regioselectivity of O-Methylation. *Mol. Pharmacol.* **2006**, *70*, 143−153.

(5) Männistö, P. T.; Kaakkola, S. Catechol-O-methyltransferase (COMT): Biochemistry, Molecular Biology, Pharmacology, and Clinical Efficacy of the New Selective COMT Inhibitors. *Pharmacol. Rev.* **1999**, *51*, 593−628.
(6) Zhang, J.; Klinman, J. P. Enzymatic Methyl Transfer: Role of an Active Site Residue in Generating Active Site Compaction That Correlates with Catalytic Efficiency. *J. Am. Chem. Soc.* **2011**, *133*, 17134−17137.
(7) Roca, M.; Martí, S.; Andrés, J.; Moliner, V.; Tuñón, I.; Bertrán, J.; Williams, I. H. Theoretical Modeling of Enzyme Catalytic Power: Analysis of "Cratic" and Electrostatic Factors in Catechol O-Methyltransferase. *J. Am. Chem. Soc.* **2003**, *125*, 7726−7737.
(8) Bai, H.-W.; Shim, J.-Y.; Yu, J.; Zhu, B. T. Biochemical and Molecular Modeling Studies of the O-Methylation of Various Endogenous and Exogenous Catechol Substrates Catalyzed by Recombinant Human Soluble and Membrane-Bound Catechol-O-Methyltransferases. *Chem. Res. Toxicol.* **2007**, *20*, 1409−1425.
(9) Lotta, T.; Vidgren, J.; Tilgmann, C.; Ulmanen, I.; Melen, K.; Julkunen, I.; Taskinen, J. Kinetics of Human Soluble and Membrane-Bound Catechol O-Methyltransferase: A Revised Mechanism and Description of the Thermolabile Variant of the Enzyme. *Biochemistry* **1995**, *34*, 4202−4210.
(10) Daly, J. W.; Axelrod, J.; Witkop, B. Dynamic Aspects of Enzymatic O-Methylation and -Demethylation of Catechols In vitro and In vivo. *J. Biol. Chem.* **1960**, *235*, 1155−1159.
(11) Creveling, C.; Morris, N.; Shimizu, H.; Ong, H.; Daly, J. Catechol O-Methyltransferase IV. Factors Affecting M- and P-Methylation of Substituted Catechols. *Mol. Pharmacol.* **1972**, *8*, 398−409.
(12) Lau, E. Y.; Bruice, T. C. Importance of Correlated Motions in Forming Highly Reactive Near Attack Conformations in Catechol O-Methyltransferase. *J. Am. Chem. Soc.* **1998**, *120*, 12387−12394.
(13) Hollman, P. C. H.; Arts, I. C. W. Flavonols, Flavones and Flavanols−Nature, Occurrence and Dietary Burden. *J. Sci. Food Agric.* **2000**, *80*, 1081−1093.
(14) Lin, A.-S.; Lin, C.-R.; Du, Y.-C.; Lübken, T.; Chiang, M. Y.; Chen, I.-H.; Wu, C.-C.; Hwang, T.-L.; Chen, S.-L.; Yen, M.-H. Acasiane A and B and Farnesirane A and B, Diterpene Derivatives from the Roots of Acacia Farnesiana. *Planta Med.* **2009**, *75*, 256−261.
(15) Comalada, M.; Ballester, I.; Bailón, E.; Sierra, S.; Xaus, J.; Gálvez, J.; Medina, F. S. d.; Zarzuelo, A. Inhibition of Pro-Inflammatory Markers in Primary Bone Marrow-Derived Mouse Macrophages by Naturally Occurring Flavonoids: Analysis of the Structure−Activity Relationship. *Biochem. Pharmacol.* **2006**, *72*, 1010−1021.
(16) Zhu, B. T.; Ezell, E. L.; Liehr, J. G. Catechol-O-Methyltransferase-Catalyzed Rapid O-Methylation of Mutagenic Flavonoids. Metabolic Inactivation as a Possible Reason for Their Lack of Carcinogenicity in vivo. *J. Biol. Chem.* **1994**, *269*, 292−299.
(17) Chen, Z.; Chen, M.; Pan, H.; Sun, S.; Li, L.; Zeng, S.; Jiang, H. Role of Catechol-O- Methyltransferase in the Disposition of Luteolin in Rats. *Drug Metab. Dispos.* **2011**, *39*, 667−674.
(18) Wright, B.; Gibson, T.; Spencer, J.; Lovegrove, J. A.; Gibbins, J. M. Platelet-Mediated Metabolism of the Common Dietary Flavonoid, Quercetin. *PLoS One* **2010**, *5*, e9673.
(19) Chen, Z. J.; Dai, Y. Q.; Kong, S. S.; Song, F. F.; Li, L. P.; Ye, J. F.; Wang, R. W.; Zeng, S.; Zhou, H.; Jiang, H. D. Luteolin Is a Rare Substrate of Human Catechol-O-Methyltransferase Favoring a Para-Methylation. *Mol. Nutr. Food Res.* **2013**, *57*, 877−885.
(20) Tsao, D.; Liu, S.; Dokholyan, N. V. Regioselectivity of Catechol O-Methyltransferase Confers Enhancement of Catalytic Activity. *Chem. Phys. Lett.* **2011**, *506*, 135−138.
(21) Bai, H.-W.; Shim, J.-Y.; Yu, J.; Zhu, B. T. Biochemical and Molecular Modeling Studies of the O-Methylation of Various Endogenous and Exogenous Catechol Substrates Catalyzed by Recombinant Human Soluble and Membrane-Bound Catechol-O-Methyltransferases†. *Chem. Res. Toxicol.* **2007**, *20*, 1409−1425.
(22) Weinert, C. H.; Wiese, S.; Rawel, H. M.; Esatbeyoglu, T.; Winterhalter, P.; Homann, T.; Kulling, S. E. Methylation of Catechins and Procyanidins by Rat and Human Catechol-O-Methyltransferase: Metabolite Profiling and Molecular Modeling Studies. *Drug Metab. Dispos.* **2012**, *40*, 353−359.
(23) Roca, M.; Andrés, J.; Moliner, V.; Tuñón, I.; Bertrán, J. On the Nature of the Transition State in Catechol O-Methyltransferase. A Complementary Study Based on Molecular Dynamics and Potential Energy Surface Explorations. *J. Am. Chem. Soc.* **2005**, *127*, 10648−10655.
(24) Kollman, P. A.; Massova, I.; Reyes, C.; Kuhn, B.; Huo, S.; Chong, L.; Lee, M.; Lee, T.; Duan, Y.; Wang, W. Calculating Structures and Free Energies of Complex Molecules: Combining Molecular Mechanics and Continuum Models. *Acc. Chem. Res.* **2000**, *33*, 889−897.
(25) Gohlke, H.; Kiel, C.; Case, D. A. Insights into Protein−Protein Binding by Binding Free Energy Calculation and Free Energy Decomposition for the Ras-Raf and Ras-RalGDS Complexes. *J. Mol. Biol.* **2003**, *330*, 891−913.
(26) Pan, X.-L.; Cui, F.-C.; Liu, W.; Liu, J.-Y. QM/MM Study on the Catalytic Mechanism of Heme-Containing Aliphatic Aldoxime Dehydratase. *J. Phys. Chem. B* **2012**, *116*, 5689−5693.
(27) Smith, G. K.; Ke, Z.; Guo, H.; Hengge, A. C. Insights into the phosphoryl transfer mechanism of cyclin-dependent protein kinases from ab initio QM/MM free-energy studies. *J. Phys. Chem. B* **2011**, *115*, 13713−13722.
(28) Li, W.; Rudack, T.; Gerwert, K.; Gräter, F.; Schlitter, J. r. Exploring the Multidimensional Free Energy Surface of Phosphoester Hydrolysis with Constrained QM/MM Dynamics. *J. Chem. Theory Comput.* **2012**, *8*, 3596−3604.
(29) *SYBYL-X*, version 1.3; software for molecular modeling from sequence through lead optimization; Tripos International: St. Louis, MO, 2011.
(30) Narwal, M.; Haikarainen, T.; Fallarero, A.; Vuorela, P. M.; Lehtiö, L. Screening and Structural Analysis of Flavones Inhibiting Tankyrases. *J. Med. Chem.* **2013**, *56*, 3507−3517.
(31) Lolli, G.; Cozza, G.; Mazzorana, M.; Tibaldi, E.; Cesaro, L.; Donella-Deana, A.; Meggio, F.; Venerando, A.; Franchin, C.; Sarno, S. Inhibition of Protein Kinase CK2 by Flavonoids and Tyrphostins. A Structural Insight. *Biochemistry* **2012**, *51*, 6097−6107.
(32) Steiner, R. A.; Kalk, K. H.; Dijkstra, B. W. Anaerobic Enzyme-Substrate Structures Provide Insight Into the Reaction Mechanism of the Copper-Dependent Quercetin 2,3-Dioxygenase. *Proc. Natl. Acad. Sci. U.S.A.* **2002**, *99*, 16625−16630.
(33) Levin, E. J.; Kondrashov, D. A.; Wesenberg, G. E.; Phillips, G. N. Ensemble Refinement of Protein Crystal Structures: Validation and Application. *Structure* **2007**, *15*, 1040−1052.
(34) Frisch, M. E.; Trucks, G.; Schlegel, H. B.; Scuseria, G.; Robb, M.; Cheeseman, J.; Scalmani, G.; Barone, V.; Mennucci, B.; Petersson, G. E.; et al. *Gaussian 09*, revision C.1; Gaussian, Inc.: Wallingford, CT, 2009.
(35) Rutherford, K.; Le Trong, I.; Stenkamp, R.; Parson, W. Crystal Structures of Human 108V and 108M Catechol *O*-Methyltransferase. *J. Mol. Biol.* **2008**, *380*, 120−130.
(36) Case, D.; Darden, T.; Cheatham, T., III; Simmerling, C.; Wang, J.; Duke, R.; Luo, R.; Walker, R.; Zhang, W.; Merz, K.; et al. *AMBER 11*; University of California: San Francisco, CA, 2010.
(37) Jorgensen, W. L.; Chandrasekhar, J.; Madura, J. D.; Impey, R. W.; Klein, M. L. Comparison of Simple Potential Functions for Simulating Liquid Water. *J. Chem. Phys.* **1983**, *79*, 926.
(38) Case, D. A.; Cheatham, T. E.; Darden, T.; Gohlke, H.; Luo, R.; Merz, K. M.; Onufriev, A.; Simmerling, C.; Wang, B.; Woods, R. J. The Amber Biomolecular Simulation Programs. *J. Comput. Chem.* **2005**, *26*, 1668−1688.
(39) Wang, J.; Wolf, R. M.; Caldwell, J. W.; Kollman, P. A.; Case, D. A. Development and Testing of a General Amber Force Field. *J. Comput. Chem.* **2004**, *25*, 1157−1174.
(40) Hornak, V.; Abel, R.; Okur, A.; Strockbine, B.; Roitberg, A.; Simmerling, C. Comparison of Multiple Amber Force Fields and Development of Improved Protein Backbone Parameters. *Proteins* **2006**, *65*, 712−725.

(41) Vidgren, J.; Svensson, L. A.; Liljas, A. Crystal Structure of Catechol O-Methyltransferase. *Nature* **1994**, *368*, 354−358.
(42) Ovaska, M.; Yliniemelä, A. A Semiempirical Study on Inhibition of Catechol O-Methyltransferase by Substituted Catechols. *J. Comput.-Aided Mol. Des.* **1998**, *12*, 301−307.
(43) Darden, T.; York, D.; Pedersen, L. Particle mesh Ewald: An N log (N) Method for Ewald Sums in Large Systems. *J. Chem. Phys.* **1993**, *98*, 10089.
(44) Ryckaert, J.-P.; Ciccotti, G.; Berendsen, H. J. Numerical Integration of the Cartesian Equations of Motion of a System with Constraints: Molecular Dynamics of *n*-Alkanes. *J. Comput. Phys.* **1977**, *23*, 327−341.
(45) Rocchia, W.; Alexov, E.; Honig, B. Extending the Applicability of the Nonlinear Poisson-Boltzmann Equation: Multiple Dielectric Constants and Multivalent Ions. *J. Phys. Chem. B* **2001**, *105*, 6507−6514.
(46) Nguyen, D. T.; Case, D. A. On Finding Stationary States on Large-Molecule Potential Energy Surfaces. *J. Phys. Chem.* **1985**, *89*, 4020−4026.
(47) Onufriev, A.; Bashford, D.; Case, D. A. Exploring Protein Native States and Large-Scale Conformational Changes with a Modified Generalized Born Model. *Proteins* **2004**, *55*, 383−394.
(48) Lightstone, F. C.; Bruice, T. C. Ground State Conformations and Entropic and Enthalpic Factors in the Efficiency of Intramolecular and Enzymatic Reactions. 1. Cyclic Anhydride Formation by Substituted Glutarates, Succinate, and 3, 6-Endoxo-Δ4-Tetrahydrophthalate Monophenyl Esters. *J. Am. Chem. Soc.* **1996**, *118*, 2595−2605.
(49) Tian, B.-X.; Eriksson, L. A. Catalytic Mechanism and Product Specificity of Oxidosqualene- Lanosterol Cyclase: A QM/MM Study. *J. Phys. Chem. B* **2012**, *116*, 13857−13862.
(50) Cerón-Carrasco, J. P.; Jacquemin, D.; Graton, J. r. m.; Thany, S.; Le Questel, J.-Y. New Insights on the Molecular Recognition of Imidacloprid with Aplysia Californica AChBP: A Computational Study. *J. Phys. Chem. B* **2013**, *117*, 3944−3953.
(51) van der Kamp, M. W.; Mulholland, A. J. Combined Quantum Mechanics/Molecular Mechanics (QM/MM) Methods in Computational Enzymology. *Biochemistry* **2013**, *52*, 2708−2728.
(52) Lundberg, M.; Sasakura, Y.; Zheng, G.; Morokuma, K. Case studies of ONIOM (DFT: DFTB) and ONIOM (DFT: DFTB: MM) for Enzymes and Enzyme Mimics. *J. Chem. Theory Comput.* **2010**, *6*, 1413−1427.